

Examination of the Feynman-Hibbs Approach in the Study of Ne_N -Coronene Clusters at Low Temperatures

Rocío Rodríguez-Cantano, Massimiliano Bartolomei, Marta I. Hernández,*

José Campos-Martínez, Tomás González-Lezana, and Pablo Villarreal

Instituto de Física Fundamental (IFF-CSIC), Serrano 123, 28006 Madrid, Spain

Ricardo Pérez de Tudela

Lehrstuhl für Theoretische Chemie, Ruhr-Universität Bochum, 44780 Bochum, Germany

Javier Hernández-Rojas and José Bretón

Departamento de Física and IUdEA,

Universidad de La Laguna, 38203 Tenerife, Spain

(Dated: August 28, 2018)

Abstract

Feynman-Hibbs (FH) effective potentials constitute an appealing approach for investigations of many-body systems at thermal equilibrium since they allow us to easily include quantum corrections within standard classical simulations. In this work we apply the FH formulation to the study of Ne_N -coronene clusters ($N = 1-4, 14$) in the 2-14 K temperature range. Quadratic (FH2) and quartic (FH4) contributions to the effective potentials are built upon Ne-Ne and Ne-coronene analytical potentials. In particular, a new corrected expression for the FH4 effective potential is reported. FH2 and FH4 cluster energies and structures -obtained from energy optimization through a basin-hopping algorithm as well as classical Monte Carlo simulations- are reported and compared with reference path integral Monte Carlo calculations. For temperatures $T > 4$ K, both FH2 and FH4 potentials are able to correct the purely classical calculations in a consistent way. However, the FH approach fails at lower temperatures, especially the quartic correction. It is thus crucial to assess the range of applicability of this formulation and, in particular, to apply the FH4 potentials with great caution. A simple model of N isotropic harmonic oscillators allows us to propose a means of estimating the cut-off temperature for the validity of the method, which is found to increase with the number of atoms adsorbed on the coronene molecule.

KEYWORDS: quantum effects, Feynman-Hibbs potentials, van der Waals clusters, polycyclic aromatic hydrocarbons

*Electronic address: marta@iff.csic.es

I. INTRODUCTION

Quantum effects are very important in a variety of many-body systems at thermal equilibrium, especially for light molecules and/or low temperatures. Among the problems of interest, we mention the behavior of water[1], the storage of small molecules in nanoporous materials[2–5] and the study of molecules trapped inside low temperature matrices, either solid[6, 7] or superfluid as in the case of He nanodroplets[8, 9]. The path-integral formulation of statistical mechanics[10] has provided the framework for the development of accurate path-integral Monte Carlo (PIMC) methods[11, 12] to study these systems. However, these methods are computationally very demanding so various approximate approaches have been developed over the years to overcome this drawback.

One of the simplest approximations is the use of Feynman-Hibbs (FH) effective potentials[13] in classical Monte Carlo (CMC) or molecular dynamics simulations. These potentials are given as a temperature- and mass-dependent expansion of the intermolecular potentials in powers of \hbar . In this way, the approach provides an easy and appealing means to include quantum corrections in a purely classical simulation. This formulation has been applied to the study of both homogeneous[14–17] and heterogeneous systems as, for instance, the sieving of H₂ and D₂ in microporous materials[5, 18–22]. In the case of homogeneous media, the validity of this method has been investigated in detail by Sesé[23, 24] from comparisons with “exact” PIMC calculations of Lennard-Jones systems (He, Ne, Ar, D₂, CH₄). Similarly, Calvo *et al*[15] found that the quadratic FH effective potential reproduces quite well the thermodynamic properties (melting temperatures, heat capacities, caloric curves, etc.) of Ne, Ar, and Xe rare gas clusters. More recently, Kowalczyk *et al*[25] assessed the FH approach for supercritical ⁴He at 10 K and concluded that the FH potentials are only suitable at low fluid densities, suggesting that previous applications to dense para-H₂ in nanoporous materials at low temperatures should be revised. It is thus interesting to investigate the validity of the FH approach for heterogeneous systems such as fluid-solid mixtures, for which specific studies are scarcer.

In this work we study the performance of the FH approach for Ne_N -coronene ($N = 1 - 4, 14$) clusters at temperatures ranging from 2 to 14 K, by comparing CMC calculations using FH potentials with the accurate PIMC method. This system can be considered as a prototype for studies of van der Waals interactions between small molecules and carbonaceous substrates[26] and, in this way, its findings may serve as a guide for future simulations of the storage of gases by new porous carbon materials[27]. In addition, the interaction between coronene and other polycyclic aromatic hydrocarbons (PAHs) with Ne atoms is interesting in connection with the spectroscopy of these molecules in Neon matrices at low temperatures (≈ 6 K), aimed to assign some bands observed from various astrophysical environments[7, 28–30].

The FH effective potentials used in the present work are built upon pairwise analytical Ne-Ne and Ne-coronene potentials and are obtained both at quadratic (\hbar^2) and quartic (\hbar^4) order, hereafter referred as FH2 and FH4 potentials, respectively. As in our recent study of He_N -coronene clusters[31], minimum energies of the bare interaction potential are obtained by means of a basin-hopping (BH) approach[32], and the optimized structures are then used as seeds for the CMC and PIMC calculations. In this work, we additionally run BH and CMC calculations with the FH2 and FH4 potentials in order to assess the extent of improvement with respect to the use of the bare potentials.

The paper is organized as follows. Section 2 presents the FH effective potentials applied to the Ne_N -coronene interaction. BH, CMC and PIMC computational methods are briefly reviewed in Section 3. Results (energies and structures at different temperatures) are reported and discussed in Section 4. Finally, concluding remarks are given in Section 5.

II. NE_N -CORONENE INTERACTION POTENTIALS

A. Bare potentials

The coronene molecule is assumed to be rigid and fixed to the reference frame. The origin of the coordinate system is placed at the coronene center of mass, with the z axis

being perpendicular to the molecular plane and the x axis being overimposed to two of the C-C bonds of this molecule. The position of i -th Ne atom is given by the Cartesian vector \mathbf{r}_i .

The total potential of the Ne_N -coronene system is given as a sum of pairwise interactions,

$$V(\mathbf{r}_1, \dots, \mathbf{r}_N) = \sum_{i=1}^N V_{\text{Ne-Cor}}(\mathbf{r}_i) + \sum_{i<j}^N V_{\text{Ne-Ne}}(\rho_{ij}), \quad (1)$$

where $V_{\text{Ne-Cor}}$ and $V_{\text{Ne-Ne}}$ are the Ne-coronene and Ne-Ne interaction potentials, respectively, and $\rho_{ij} = |\mathbf{r}_i - \mathbf{r}_j|$ is the distance between i -th and j -th Ne atoms.

The Ne-Ne potential is represented by the Improved Lennard-Jones (ILJ) formula[33]:

$$V_{\text{Ne-Ne}}(\rho) = \frac{\varepsilon}{m(\rho) - 6} \left[6 \left(\frac{\rho}{\rho_e} \right)^{-m(\rho)} - m(\rho) \left(\frac{\rho}{\rho_e} \right)^{-6} \right], \quad (2)$$

where ε is the well depth, ρ_e is the equilibrium distance, and

$$m(\rho) = \gamma + 4 \left(\frac{\rho}{\rho_e} \right)^2. \quad (3)$$

Although Eq. 2 is more involved than the standard Lennard-Jones expression, the ILJ potential gives a more realistic representation of both the size repulsion and the long-range dispersion attraction, as discussed elsewhere[33]. Values of the parameters ε , ρ_e and γ have been taken from Ref.[33] and are given in Table I.

The Ne-coronene potential is given as a sum of atom-bond pairwise contributions[34, 35],

$$V_{\text{Ne-Cor}}(\mathbf{r}) = \sum_k U_k(\rho_k, c_k), \quad (4)$$

where k runs for the number of bonds (C-C and C-H) in coronene, ρ_k is the distance between the atom and the bond center and $c_k = \cos(\theta_k)$, θ_k being the Jacobian angle describing the orientation of Ne relative to the bond axis. Both ρ_k and c_k are functions of the Ne position (\mathbf{r}) as well as of the location and orientation of the bond k . Geometrical parameters of coronene are as in Ref. [35]. The atom-bond pair potential U_k is represented, as in Ne-Ne,

by an ILJ formula (Eq.2), with the special feature that the well depth and the equilibrium distance vary with c_k as[34]

$$\begin{aligned}\varepsilon(c_k) &= \varepsilon^\perp + (\varepsilon^\parallel - \varepsilon^\perp) c_k^2 \\ \rho_e(c_k) &= \rho_e^\perp + (\rho_e^\parallel - \rho_e^\perp) c_k^2,\end{aligned}\tag{5}$$

where ε^\perp (ε^\parallel) and ρ_e^\perp (ρ_e^\parallel) are the well depth and equilibrium distance for the perpendicular (parallel) orientation of the atom with respect to the bond. These parameters were initially estimated from the polarizability of the interacting partners, and subsequently fine-tuned from the comparison with benchmark high level *ab initio* calculations involving large basis sets[35]. Their values are listed in Table I for the two types of the involved bonds, C-C and C-H.

It is worth noting that the atom-bond additive representation takes into consideration three-body effects since it explicitly makes use of the components of the bond polarizability tensor and in the end it provides a good estimation of the total (coronene) molecular polarizability. On the other hand, the present model neglects three-body effects arising between two rare gas atoms and a third body (either Ne or coronene), which however are expected to be negligible for the investigated equilibrium geometries.

B. Feynman-Hibbs effective potentials

The FH effective potentials for an A-B interacting system are obtained from the following gaussian average of the V_{AB} potential [13, 23]

$$V_{AB}^{\text{FH}}(\mathbf{r}) = \left(\frac{6\mu}{\pi\hbar^2\beta} \right)^{3/2} \int d\mathbf{u} V_{AB}(\mathbf{r} + \mathbf{u}) \exp\left(-\frac{6\mu}{\beta\hbar^2}u^2\right),\tag{6}$$

where \mathbf{r} is the vector joining A and B, μ is the A-B reduced mass, and $\beta = 1/k_B T$, k_B being the Boltzmann constant. Eq.6 is based on a variational treatment of the path-integral and involves the neglect of exchange effects[23]. Closed expressions of the FH potential

are obtained upon a Taylor expansion of $V_{AB}(\mathbf{r} + \mathbf{u})$ around the vector \mathbf{r} in powers of the Cartesian components of \mathbf{u} and solving the corresponding integrals of Eq.6. We have[24]

$$V_{AB}^{\text{FH}(2p)}(\mathbf{r}) = \sum_{n=0}^p \frac{1}{n!} \left(\frac{\beta \hbar^2}{24\mu} \right)^n \nabla^{2n} [V_{AB}(\mathbf{r})], \quad (7)$$

where $\nabla^0 = 1$ and $p = 0, 1, 2$ correspond to the bare, quadratic (FH2) and quartic (FH4) potentials, respectively. Note that the integral of Eq. 6 vanishes for the contributions involving odd powers of the components of \mathbf{u} . It can be seen that at high temperatures the effective potentials tend to the bare potential and the classical regime is correctly recovered. However, as temperature tends to zero these potentials become unphysically high, which will inevitably impose limits to the model.

In the case of the Ne-Ne interaction, $V_{AB}(\mathbf{r})$ depends on $|\mathbf{r}| \equiv \rho$ and the FH2 potential becomes

$$V_{\text{Ne-Ne}}^{\text{FH2}}(\rho) = V_{\text{Ne-Ne}}(\rho) + \frac{\hbar^2 \beta}{24\mu} \left(V_{\text{Ne-Ne}}''(\rho) + \frac{2}{\rho} V_{\text{Ne-Ne}}'(\rho) \right), \quad (8)$$

where $V_{\text{Ne-Ne}}$ is the potential of Eq.2 and $V_{\text{Ne-Ne}}'$ and $V_{\text{Ne-Ne}}''$ are their first and second derivatives, respectively, with respect to ρ .

The quartic Ne-Ne effective potential (FH4) writes

$$V_{\text{Ne-Ne}}^{\text{FH4}}(\rho) = V_{\text{Ne-Ne}}^{\text{FH2}} + \frac{1}{2} \left(\frac{\hbar^2 \beta}{24\mu} \right)^2 \left(V_{\text{Ne-Ne}}''''(\rho) + \frac{4}{\rho} V_{\text{Ne-Ne}}'''(\rho) \right), \quad (9)$$

where, analogously, $V_{\text{Ne-Ne}}'''$ and $V_{\text{Ne-Ne}}''''$ are the third and fourth derivatives of $V_{\text{Ne-Ne}}$ with respect to ρ .

It is worth pointing out that Eq. 9 differs from previously published expressions[18, 19, 21, 25], which we believe are incorrect. More details are provided in the Appendix.

The form of the Ne-coronene FH2 potential is more complicated because the atom-bond potentials U_k of Eq.4 depend both on the distance to the bond center ρ_k and the cosine of the Jacobian angle, c_k . The result is

$$V_{\text{Ne-Cor}}^{\text{FH2}}(\mathbf{r}) = V_{\text{Ne-Cor}}(\mathbf{r}) + \frac{\hbar^2\beta}{24m_{\text{Ne}}} \sum_k \left\{ \frac{\partial^2 U_k}{\partial \rho_k^2} + \frac{2}{\rho_k} \frac{\partial U_k}{\partial \rho_k} + \frac{(1-c_k^2)}{\rho_k^2} \frac{\partial^2 U_k}{\partial c_k^2} - \frac{2c_k}{\rho_k^2} \frac{\partial U_k}{\partial c_k} \right\}. \quad (10)$$

Note that in Eq.10 the Ne mass is written instead of the reduced mass of Ne-coronene. We have made this choice because the coronene molecule is fixed to the reference frame and it is thus assumed that it has an infinite mass.

We have found that the contribution to $V_{\text{Ne-Cor}}^{\text{FH2}}$ due to the derivatives of U_k with respect to c_k are very small. To simplify the calculations, we have assumed that the contributions from these derivatives to the terms of \hbar^4 order are negligible. In this way, the FH4 potential is written as

$$V_{\text{Ne-Cor}}^{\text{FH4}}(\mathbf{r}) = V_{\text{Ne-Cor}}^{\text{FH2}}(\mathbf{r}) + \frac{1}{2} \left(\frac{\hbar^2\beta}{24m_{\text{Ne}}} \right)^2 \sum_k \left\{ \frac{\partial^4 U_k}{\partial \rho_k^4} + \frac{4}{\rho_k} \frac{\partial^3 U_k}{\partial \rho_k^3} \right\}. \quad (11)$$

Nevertheless, the exact expression for the correction of \hbar^4 order is given in Eq. 25, and it has been additionally checked that the contribution to that equation of the derivatives of the atom-bond potential with respect to c_k is negligible.

More details about the derivation of Eqs. 8-11 are provided in the Appendix. All the required derivatives of the ILJ functions were obtained analytically as well as the gradients of the potentials of Eqs.8-11 (needed for the application of the BH algorithm referred below). In any case, recent advances in techniques of automatic differentiation[36] might prove advantageous for this kind of simulations.

The Ne-Ne bare potential as well as the FH2 and FH4 ones at 6 K are presented in Fig. 1. The ILJ form of the bare potential is very realistic, as we have compared it with the Tang-Toennies potential[37] and found that both potentials would appear as indistinguishable in Fig. 1. Indeed, the well depth and equilibrium distance of the Tang-Toennies potential are 3.646 meV and 3.090 Å, very close to the values of Table I. On the other hand, it can be seen in Fig. 1 that the FH corrections significantly modify the bare potential, the effective

potentials being more “repulsive”: the equilibrium distance changes from 3.09 to 3.24 (3.28) Å and the well depth, from 3.66 to 3.03 (2.84) meV, as one goes from the bare to the FH2 (FH4) potentials, respectively.

The corresponding potentials for Ne-coronene are shown in Fig.2 as functions of the y coordinate, while z and x are fixed at the absolute minimum of the classical potential (at 3.21 and 0 Å, respectively). Again, it can be seen that the effect of the quadratic correction is non negligible, for instance, the minimum energy moves from -27.83 (bare potential) to -25.68 meV (FH2 potential) but, on the other hand, the FH4 potential is very close to the FH2 one.

III. CLASSICAL AND QUANTUM-MECHANICAL CALCULATIONS

A. General procedure and notation

In this work we compare the performance of the Ne_N -coronene FH2 and FH4 effective potentials with that of the bare interaction potentials. First, we will study the equilibrium geometries of these clusters by means of the BH approach. The corresponding calculations are denoted by BH, BH-FH2 and BH-FH4 for the bare, FH2 and FH4 potentials, respectively. Note that, while the BH calculations are independent of the temperature, BH-FH2 and BH-FH4 must be repeated for the different temperatures of the study. The BH equilibrium geometries are used as initial configurations of the CMC calculations at each temperature, which will be denoted as CMC, CMC-FH2 and CMC-FH4, for the bare, FH2 and FH4 potentials, respectively. The resulting energies and configurations are compared with the PIMC calculations, where just the bare interaction potential is employed.

For the BH calculations using the bare interaction potential, the zero point energy (ZPE) was also computed within the harmonic approximation and added to the BH equilibrium energies (details can be found in Ref.[31]). This is a convenient estimation of the quantum effects of the system when the thermal effects become small, as will be discussed in Section IV. These calculations are denoted by BH+ZPE.

B. BH minimization

Likely candidates for the global potential energy minima of Ne_N -coronene clusters were located using the BH scheme [32], which is also known as the “Monte Carlo plus energy minimization” approach of Li and Scheraga [38]. This method transforms the potential energy surface into a collection of basins and explore them by hopping between local minima. This technique has been used successfully for both neutral [32, 39, 40] and charged atomic and molecular clusters [41–46], along with many other applications.[47] In the size range considered here the global optimization problem is feasible at a reasonable computational cost. A total of 5 runs of 5×10^4 BH steps each were performed for all clusters sizes. The global minimum was generally found in fewer than 10^4 BH steps. The optimization temperature was chosen between 8 and 10 K.

C. PIMC and CMC calculations

Details of the PIMC method employed here can be found in our study on He_N -coronene clusters [31] and in previous literature[11, 48–51]. The basic assumption involves expressing the density matrix at a temperature T as a product of M density matrices at higher temperatures MT :

$$\rho(\mathcal{R}_0, \mathcal{R}_M; \beta) = \int d\mathcal{R}_1 \dots d\mathcal{R}_{M-1} \prod_{\alpha=0}^{M-1} \rho(\mathcal{R}_\alpha, \mathcal{R}_{\alpha+1}; \eta), \quad (12)$$

where $\eta = \beta/M$. \mathcal{R}_α is the vector which collects the $3N$ positions of the N Ne atoms: $\mathcal{R}_\alpha \equiv \{\mathbf{r}_1^\alpha, \dots, \mathbf{r}_N^\alpha\}$, being \mathbf{r}_i^α the position vector of the i -th Ne atom at the time *slice* or *imaginary* time α . The total Hamiltonian \hat{H} of the system with the coronene molecule fixed to the origin of coordinates can be written as:

$$\hat{H} = -\frac{\hbar^2}{2m_{\text{Ne}}} \sum_{i=1}^N \nabla_i^2 + V(\mathcal{R}). \quad (13)$$

where V is the interaction potential of Eq.1.

The internal energy is obtained by means of the virial estimator [52, 53] as:

$$\langle E(T) \rangle = \frac{3N}{2\beta} - \left\langle \frac{1}{2M} \sum_{\alpha=0}^{M-1} \sum_{i=1}^N (\mathbf{r}_i^\alpha - \mathbf{r}_i^C) \cdot \mathbf{F}_i^\alpha - \frac{1}{M} \sum_{\alpha=0}^{M-1} V(\mathcal{R}_\alpha) \right\rangle. \quad (14)$$

where $\mathbf{r}_i^C = M^{-1} \sum_{\alpha=0}^{M-1} \mathbf{r}_i^\alpha$ is the centroid of the i th particle and \mathbf{F}_i^α is the force experienced by the i particle on the α slice. The integration is carried out via a Metropolis Monte Carlo algorithm, as an average over a number of paths $\{\mathcal{R}_1, \mathcal{R}_2, \dots, \mathcal{R}_M, \mathcal{R}_{M+1}\}$ sampled according to a probability density proportional to the factorized product of M density matrices of Eq.12. Exchange effects are neglected. The number of beads vary between $M=1$ (for the CMC, CMC-FH2 and CMC-FH4 calculations) to a maximum of 150 for the lowest temperature PIMC simulations. Depending on M , the number of steps varies between 10^5 to 10^7 . The staging sampling method has been employed[54] involving a number of eight beads in each movement for the PIMC simulations. The final average energy is obtained by extrapolation to the $M \rightarrow \infty$ following a parabolic law[55, 56].

IV. RESULTS AND DISCUSSION

A. Cluster energies and structures at 6 K

Before tackling the study of the FH approximation as a function of the temperature, we start presenting results at 6 K, an intermediate value in the range addressed here and in coincidence with the temperature of various experiments on PAHs isolated in Ne matrices[7, 29, 30].

In Table II, energies of various Ne_N -coronene clusters, $N=1-4$ and 14, at 6 K as obtained from the BH and CMC approaches and using the bare, FH2 and FH4 effective potentials are reported and compared with the PIMC results. Various arrangements (or “isomers”) (n_a, n_b) are examined for each number of Ne atoms, where n_a and n_b refer to the number of atoms placed above and below the coronene plane, respectively. It can be seen that both the BH and the CMC energies tend to the PIMC energies as one goes from using the bare to

the FH2 and FH4 potentials. However, given the difference between the BH and the CMC energies, it is clear that thermal effects are non negligible at this temperature so, among all the calculations, the CMC-FH4 energies are the ones giving the closest agreement with the reference PIMC results. In addition, notice that CMC-FH4 agrees with PIMC as to which is the most stable isomer (n_a, n_b) for a given cluster size N . For example, for $N = 4$, the most stable arrangement within the FH4 potential is the (3,1) one, in agreement with the PIMC calculation, whereas (4,0) gives the absolute minimum when using the bare and FH2 potentials. This result can be explained by a more repulsive character of Ne-Ne interaction when it is considered at the FH4 level (Fig.1), thus making an arrangement with a larger density of Ne atoms relatively less stable (as the (4,0) one).

Also from Table II, it is worth mentioning that the addition of the ZPE to the BH energies gives a fair agreement with the PIMC energies, and that the BH+ZPE calculations correctly predict the relative stability of the different isomers for a given N .

Computation of the energies per atom helps us to quantify the performance of the FH approach. Results are depicted in Fig.3, where it is clear the improvement of the CMC-FH energies with respect to the CMC ones. In more detail, note that, for a given N , the differences between the CMC and PIMC energies are larger for those clusters having a larger number of atoms on a given side of the molecule. In this case, quantum effects increase because the number of effective Ne-Ne interactions increases as well (interactions between atoms sitting on different sides of the molecule are negligible). For example, for (3,0), with three effective Ne-Ne interactions, the relative error of the CMC calculation is 14 %, whereas for the (2,1) cluster, with just one Ne-Ne interaction, the error reduces to 11 %. The FH2 and FH4 potentials certainly amend the classical result, although the errors are also larger when the number of interacting atoms increase. Indeed, the errors of the CMC-FH2 calculation are 5 % and 2 % for the (3,0) and (2,1) clusters, respectively. It is important to mention that both Ne-Ne and Ne-coronene interactions contribute significantly to the quantum corrections: for the (3,0) cluster, 24 % and 76 % of the FH2 correction (computed at the corresponding optimal geometry) are due to Ne-Ne and Ne-coronene, respectively,

whereas these numbers become 12 % and 88% in the case of the (2,1) arrangement.

Besides increasing the overall energies, there are some changes in the geometries of the Ne_N -coronene clusters when the interaction potentials are modified. Probability densities as functions of the coordinates parallel to the coronene plane, $\mathcal{D}(x, y)$, as obtained from PIMC, CMC-FH4 and CMC, are shown in Fig.4 for (7,7) Ne_{14} -coronene at 6 K (results for the FH2 potential are not shown as they are quite close to the FH4 ones). These plots have been obtained by means of a histogramming procedure on the x and y coordinates, accumulating the probability density along the z coordinate. For each side of the molecule, one Ne atom is placed above the central hollow, while the other six atoms are located near the borders of the outer hexagons. The distributions from the different calculations are quite similar. However, it can be noticed that the peaks of the PIMC and CMC-FH4 probability densities are somewhat wider and that the average distance between those peaks is slightly larger than in the case of the CMC calculation. These features can be further examined by means of the one-dimensional distribution $\mathcal{D}([x^2 + y^2]^{1/2})$ as shown in Fig.5 (it is computed by accumulating the probability density $\mathcal{D}(x, y)$ along the angle φ given by $\tan \varphi = y/x$). The CMC-FH4 distribution is in better agreement with the PIMC calculations than the purely classical one. Fig.5 also depicts the distance of the outer Ne atoms with respect to the coronene symmetry axis (z) as obtained from the BH and BH-FH4 optimized geometries, and it can be seen that these positions coincide with the maxima of the corresponding CMC distributions. The FH4 potential involves larger equilibrium distances than the bare potential (for instance, see Fig. 1), a feature that can explain the shift in the peak position of the CMC-FH4 with respect to the CMC one. The peak of the PIMC distribution is in the middle, suggesting that the FH4 potential is overestimating this effect.

B. Temperature dependence of the cluster energies

Further insight is gained into the FH approach by studying the cluster energies as functions of the temperature for the different cluster sizes. In Fig.6, the behavior of the (1-4,

0) and (7,7) cluster energies as obtained from the different potentials and methods is tested against PIMC in the temperature range 2-14 K. To make a more coherent comparison, the energies have been shifted by the minimum energy (BH) and divided by the number of atoms,

$$\tilde{E}(T) = \frac{E(T) - E^{\text{BH}}}{N}. \quad (15)$$

Although not all of the $(n_a=1-4,0)$ arrangements correspond to the absolute minimum energy (see Table II), we have chosen this sequence in order to study the FH approach as a function of the number of Ne atoms over a given face of the molecule.

In the higher temperature range of Fig. 6 ($T > 6$ K) the three CMC calculations give a monotonous increase of the cluster energies with the temperature, in agreement with the behavior of the PIMC energies. In this region, the CMC-FH2 method considerably improves the cluster energies with respect to the CMC calculations, while the CMC-FH4 calculation just adds a small correction to the CMC-FH2 results. This is illustrated in Table III, where the relative errors of the three CMC calculations are listed at $T = 10$ K. Note that “unshifted” energies were taken for the calculation of the relative errors (i.e., E instead of \tilde{E}). Note that the CMC errors rise with the number of Ne atoms, as already discussed above. It can also be seen from the Table that the CMC-FH2 and CMC-FH4 calculations roughly halve the CMC errors independently of the number of Ne atoms. Therefore, although the FH2 and FH4 potentials do not provide a perfect agreement with the PIMC energies, they do introduce quantum corrections in a steady way.

As temperature decreases ($T \lesssim 6$ K), quantum effects become dominant over the thermal ones and a different behavior of the methods is evident. On the one hand, the slope of the PIMC energies is modified to reach a horizontal asymptote given by the ZPE of the system. The CMC energies, on the other hand, tend (linearly) to zero, deviating considerably from the quantum calculation. Finally, the CMC-FH2 and CMC-FH4 energies reach a minimum at about 6 K and rapidly increase as temperature decreases, also in contrast with

the correct behavior given by PIMC. In this way, the effective potentials are not adequate for temperatures below $\lesssim 4$ K.

The functional dependence of the CMC-FH2 (CMC-FH4) energies with the temperature can be easily understood as soon as it is realized that they are almost equal to the sum of the BH-FH2 (BH-FH4) and the CMC energies, which account for quantum and thermal effects, respectively. In other words, in the present system, the behavior of the CMC-FH2 (CMC-FH4) energies is identical to that of CMC except for the (temperature-dependent) modification of the local minimum energy due to the effective FH2 (FH4) potentials.

It is also worthwhile to note that the slope of all the CMC curves of Fig. 6 is roughly $3 k_B$, in agreement with a model of N classical harmonic oscillators in a three-dimensional (3D) space. In addition, the PIMC energies at low temperatures are in a fairly good agreement with the ZPE computed here within the harmonic approximation (dotted lines in Fig. 6). In this way, we have tested a model of N 3D isotropic harmonic oscillators against present calculations. It is assumed that each of the N Ne atoms moves under an effective potential $V_{\text{har}}(r) = m_{\text{Ne}}\omega_N r^2/2$, where ω_N is a characteristic frequency which varies with N . Its value is obtained from equating the computed ZPE per atom to $3\hbar\omega_N/2$. In this way, the “average interaction” undergone by each atom -which depends on the interaction with both the molecular substrate and the remaining atoms in the cluster- is approximated by an isotropic harmonic potential. Within this model, the quantum mechanical average energy per atom is [57]

$$\tilde{E}_{\text{har}}^{\text{q}}(T) = \frac{3}{2} \hbar\omega_N \coth \frac{\hbar\omega_N}{2k_B T}, \quad (16)$$

to be compared with the PIMC energy. Applying Eq. 7 to the harmonic potential V_{har} , the FH2 potential is

$$\tilde{E}_{\text{har}}^{\text{BH-FH2}}(T) = \frac{1}{8} \frac{(\hbar\omega_N)^2}{k_B T}, \quad (17)$$

which will be associated with the BH-FH2 energy. Note that the FH4 potential is identical to the FH2 one within the present harmonic approximation. The FH2 thermal energy per

atom is obtained by adding $3k_B T$,

$$\tilde{E}_{\text{har}}^{\text{CMC-FH2}}(T) = \tilde{E}_{\text{har}}^{\text{BH-FH2}}(T) + 3k_B T, \quad (18)$$

which will be related to the CMC-FH2 energies. Results are shown in Fig. 7 for the (2,0) and (4,0) clusters. Although anisotropy and anharmonicity effects should probably be added to attain a more quantitative agreement, the model energies compare fairly well with the computed ones and, in this way, this simple model does provide an adequate zero-order description of the behavior of these clusters.

C. Applicability of the FH2 and FH4 effective potentials

The results of Fig. 6 indicate that both FH2 and FH4 potentials are useful for $T > 4$ K. It is evident, however, that below this temperature the CMC energies computed with these potentials deviate considerably from the reference PIMC behavior, and that this effect is more pronounced for the quartic (FH4) potential. This is in accord with the indication of Ref. [16] that the FH2 approximation is valid whenever the next term in the expansion (the quartic one) remains much smaller than the quadratic term. In a more detailed study of Ne and ^4He Lennard-Jones systems, Sesé[24] found that the FH2 potential generally performs better than the FH4 one. In this work, we have found that the FH4 potential is useful just in a narrow range of temperatures (around 6 K), since at larger temperatures its corrections become negligible whereas at lower temperatures it worsens the FH2 estimations.

It is thus important to determine the temperature range of validity of these effective potentials as they can lead to erroneous results when applied below a critical temperature T^* . Sesé has found that, for relatively low densities, this temperature can be deduced from the condition $\lambda_B/\sigma < 0.5$, where $\lambda_B = \hbar\sqrt{2\pi/mk_B T^*}$ is the thermal de Broglie wavelength and σ is the Lennard-Jones collision diameter. Here, taking $\sigma = 2.76 \text{ \AA}$ (the diameter of the Ne-Ne ILJ potential), we obtain $T^* \approx 8$ K. This is a somewhat strict condition in view of the specific results of this work.

Based in the model of isotropic harmonic oscillators described above, we have found a simple means of estimating the critical temperature T^* that might be extrapolated to related systems where PIMC calculations would become too time-consuming. This temperature is defined as the crossing between the approximate ($\tilde{E}_{\text{har}}^{\text{CMC-FH2}}$) and the quantum ($\tilde{E}_{\text{har}}^{\text{q}}$) energies. Given that at low temperatures $\tilde{E}_{\text{har}}^{\text{q}}(T) \approx \frac{3}{2}\hbar\omega_N$, the ZPE per atom of the system, a simple quadratic equation follows, whose lowest root is

$$T^* = \frac{3}{2}\hbar\omega_N \left(\frac{1 - \sqrt{1/3}}{6 k_B} \right). \quad (19)$$

The resulting temperatures range from $T^* = 2.8$ to 4.8 K as we go from the (1,0) to the (7,7) cluster, respectively. It is worth noting that this model correctly takes into account the shift of T^* with the number of rare gas atoms (density), as found for other systems[23, 25]. Indeed, T^* is proportional to the ZPE per atom, which increases with the number of Ne atoms, as can be seen in Fig. 6. This trend is possibly due to a rise of the frequencies of the average interaction undergone by each Ne atom as the number of rare gas atoms surrounding it increases.

V. CONCLUDING REMARKS

The Feynman-Hibbs (FH) approach has been applied to the study of Ne_N -coronene clusters ($N = 1-4, 14$) at low temperatures ($T = 2-14$ K) and using realistic analytical potentials. The suitability of the quadratic (FH2) and quartic (FH4) effective potentials has been investigated by comparing basin-hopping (BH) optimizations and classical Monte Carlo (CMC) calculations of cluster energies and structures with benchmark path-integral Monte Carlo (PIMC) calculations.

For $T > 4$ K it is found that, although there is not a perfect agreement with the PIMC calculations, the effective potentials significantly improve the purely classical calculations. Quantum effects -which are significant and due to both Ne-Ne and Ne-coronene interactions- are partially corrected by the FH potentials in a reliable way. In particular, the FH4 ap-

proach at 6 K correctly predicts the most stable structure over a set of energetically close local minima, and tends to emulate the PIMC probability distributions (although these distributions do not vary as much as the energies).

For lower temperatures $T \lesssim 4$ K, where zero-point energy (ZPE) effects dominate over thermal ones, the FH formulation fails to reproduce the dependence of the PIMC energies with the temperature, while the BH+ZPE approximation does reproduce well the PIMC results. In particular, the FH4 potential, which generally improves the results of the FH2 potentials at higher temperatures, deviates more dramatically from the correct results than the FH2 approach. Therefore, the quartic effective potential, which has been recently employed in simulations of the diffusion of light molecules in nanoporous materials[18, 21, 22], should be applied with extreme caution.

We believe that further investigations of the performance of these effective potentials are worthwhile as they allow us to include quantum effects (i.e., ZPE effects) into classical simulations in a straightforward manner. For instance, it would be interesting to explore in detail the performance of these potentials for dynamical processes -such as the transmission of atoms through nanoporous membranes[58]- using Path Integral Molecular Dynamics approaches as benchmark quantum simulations.

VI. APPENDIX: DERIVATION OF THE FEYNMAN-HIBBS EFFECTIVE POTENTIALS

In this paragraph we give a more detailed account of the derivation of the quadratic (FH2) and quartic (FH4) effective potentials for the interaction potentials of this study (Eqs. 8-11). Since these potentials are of the type $V(\rho)$ or $V(\rho, \cos \theta)$, it is convenient to consider the operators of Eq.7 in spherical coordinates. In particular, the Laplacian is given, in terms of $\mathbf{r} \equiv (r, \cos \theta, \phi)$, as

$$\nabla^2 = \frac{\partial^2}{\partial r^2} + \frac{2}{r} \frac{\partial}{\partial r} + \frac{1}{r^2} \left((1 - c^2) \frac{\partial^2}{\partial c^2} - 2c \frac{\partial}{\partial c} + \frac{1}{(1 - c^2)} \frac{\partial^2}{\partial \phi^2} \right), \quad (20)$$

where $c = \cos \theta$.

To apply Eq.7, we use the property of invariance of the Laplacian operator under any translation or rotation in the three-dimensional space. In the case of the Ne-Ne interaction, the origin of the coordinate system is displaced to coincide with one of the atoms, and, since $V_{\text{Ne-Ne}}$ only depends on the radial distance ρ ,

$$\nabla^2 V_{\text{Ne-Ne}} = \frac{d^2 V_{\text{Ne-Ne}}}{d\rho^2} + \frac{2}{\rho} \frac{dV_{\text{Ne-Ne}}}{d\rho}, \quad (21)$$

leading to the FH2 correction of Eq.8.

For the Ne-coronene interaction, taking into account Eq. 4

$$\nabla^2 V_{\text{Ne-Cor}}(\mathbf{r}) = \sum_k \nabla^2 U_k(\rho_k, c_k). \quad (22)$$

For every bond k , $\nabla^2 U_k$ can be easily performed after a transformation from the original Cartesian system to a new one where the origin is at the bond center and the z axis is aligned with the bond axis. In this way, ρ_k and c_k coincide with the radial distance and the cosine of the polar angle of the new reference system and, taking into account Eq.20 and the independence of the potential with respect to the azimuthal angle,

$$\nabla^2 U_k = \frac{\partial^2 U_k}{\partial \rho_k^2} + \frac{2}{\rho_k} \frac{\partial U_k}{\partial \rho_k} + \frac{1}{\rho_k^2} \left((1 - c_k^2) \frac{\partial^2 U_k}{\partial c_k^2} - 2c_k \frac{\partial U_k}{\partial c_k} \right), \quad (23)$$

which can be readily related to Eq. 10.

To obtain the FH4 potential of the Ne-Ne interaction, the ∇^4 operator from Eq. 7 is applied to $V_{\text{Ne-Ne}}$ as

$$\begin{aligned} \nabla^4 V_{\text{Ne-Ne}} &= \left(\frac{d^2}{d\rho^2} + \frac{2}{\rho} \frac{d}{d\rho} \right) \left(\frac{d^2 V_{\text{Ne-Ne}}}{d\rho^2} + \frac{2}{\rho} \frac{dV_{\text{Ne-Ne}}}{d\rho} \right) \\ &= \frac{d^4 V_{\text{Ne-Ne}}}{d\rho^4} + \frac{4}{\rho} \frac{d^3 V_{\text{Ne-Ne}}}{d\rho^3}, \end{aligned} \quad (24)$$

an expression which can be immediately identified with the FH4 corrections of Eq.9.

At this point, it is worthwhile noting that other authors[18, 19, 21, 25] have reported an extra term, specifically $\frac{15}{\rho^3} \frac{dV}{d\rho}$, in the formal expressions of the FH4 potentials (Eq. 2 of Ref. [18] for example). We have checked that the contributions depending on other derivatives of the potential out of the third and fourth derivatives are canceled out in the calculation of $\nabla^4 V$, and therefore, that the correct FH4 potential expression is that given by Eq. 9 of this work.

Finally, the ∇^4 operator applied to the atom-bond potential $U_k(\rho_k, c_k)$ is

$$\begin{aligned} \nabla^4 U_k = & \frac{\partial^4 U_k}{\partial \rho_k^4} + \frac{4}{\rho_k} \frac{\partial^3 U_k}{\partial \rho_k^3} + \frac{2}{\rho_k^2} \left[(1 - c_k^2) \frac{\partial^4 U_k}{\partial \rho_k^2 \partial c_k^2} - 2c_k \frac{\partial^3 U_k}{\partial \rho_k^2 \partial c_k} \right] \\ & + \frac{1}{\rho_k^4} \left[(1 - c_k^2)^2 \frac{\partial^4 U_k}{\partial c_k^4} - 8c_k(1 - c_k^2) \frac{\partial^3 U_k}{\partial c_k^3} - 4(1 - 3c_k^2) \frac{\partial^2 U_k}{\partial c_k^2} \right]. \end{aligned} \quad (25)$$

Eq. 11 is readily obtained once all the derivatives with respect c_k are neglected, as already discussed elsewhere.

Acknowledgments

The work has been funded by Spanish MINECO grants FIS2013-48275-C2-1-P, FIS2014-51993-P, and FIS2013-41532-P. R. R.-C. thanks support from FIS2013-48275-C2-1-P. Allocation of computing time by CESGA (Spain) and support by the COST-CMTS Action CM1405 ‘‘Molecules in Motion (MOLIM)’’ are also acknowledged.

-
- [1] F. Paesani and G. A. Voth, *J. Phys. Chem. B* **113**, 5702 (2009).
 - [2] D. P. Broom and K. M. Thomas, *MRS Bulletin* **38**, 412 (2013).
 - [3] J. Cai, Y. Xing, and X. Zhao, *RSC Advances* **2**, 8579 (2012).
 - [4] A. Martínez-Mesa, L. Zhechkov, S. N. Yurchenko, T. Heine, G. Seifert, and J. Rubayo-Soneira, *J. Phys. Chem. C* **116**, 19543 (2012).
 - [5] T. X. Nguyen, H. Jobic, and S. K. Bhatia, *Phys. Rev. Lett.* **105**, 085901 (2010).

- [6] M. Bahou, Y. J. Wu, and Y. P. Lee, *Angew. Chem. Int. Ed.* **53**, 1021 (2015).
- [7] I. Garkusha, A. Nagy, J. Fulara, M. F. Rode, A. L. Sobolewski, and J. P. Maier, *J. Phys. Chem. A* **117**, 351 (2013).
- [8] S. Yang and A. M. Ellis, *Chem. Soc. Rev.* **42**, 472 (2013).
- [9] S. Szalewicz, *Int. Rev. Phys. Chem.* **27**, 273 (2008).
- [10] R. P. Feynman, *Statistical Mechanics* (Benjamin, New York, 1972).
- [11] D. M. Ceperley, *Rev. Mod. Phys.* **67**, 279 (1995).
- [12] C. Chakravarty, *Int. Rev. Phys.* **16**, 421 (1997).
- [13] R. P. Feynman and A. Hibbs, *Quantum Mechanics and Path-Integrals* (McGraw-Hill, New York, 1965).
- [14] B. Guillot and Y. Guissani, *J. Chem. Phys.* **108**, 10162 (1998).
- [15] F. Calvo, J. P. K. Doye, and D. J. Wales, *J. Chem. Phys.* **114**, 7312 (2001).
- [16] N. Tchouar, F. Ould-Kaddour, and D. Levesque, *J. Chem. Phys.* **121**, 7326 (2004).
- [17] M. Abbaspour and Z. Borzouie, *Fluid Phase Equilibria* **379**, 167 (2014).
- [18] A. V. A. Kumar and S. K. Bhatia, *Phys. Rev. Lett.* **95**, 245901 (2005).
- [19] A. V. A. Kumar, H. Jobic, and S. K. Bhatia, *J. Phys. Chem. B* **110**, 16666 (2006).
- [20] D. Noguchi, H. Tanaka, A. Kondo, H. Kajiro, H. Noguchi, T. Ohba, H. Kanoh, and K. Kaneko, *J. Am. Chem. Soc.* **130**, 6367 (2008).
- [21] D. Liu, W. Wang, J. Mi, C. Zhong, Q. Yang, and D. Wu, *Ind. Eng. Chem. Res.* **51**, 434 (2012).
- [22] C. I. Contescu, H. Zhang, R. J. Olsen, E. Mamontov, J. R. Morris, and N. C. Gallego, *Phys. Rev. Lett.* **110**, 236102 (2013).
- [23] L. M. Sesé, *Mol. Phys.* **81**, 1297 (1994).
- [24] L. M. Sesé, *Mol. Phys.* **85**, 931 (1995).
- [25] P. Kowalczyk, L. Brualla, P. A. Gauden, and A. P. Terzyk, *Phys. Chem. Chem. Phys.* **11**, 9182 (2009).
- [26] Y. Jiao, A. Du, M. Hankel, and S. C. Smith, *Phys. Chem. Chem. Phys.* **15**, 4832 (2013).
- [27] M. Bartolomei, E. Carmona-Novillo, and G. Giorgi, *Carbon* **95**, 1076 (2015).
- [28] C. Joblin, L. d'Hendecourt, A. Léger, and D. Défourneau, *Astron. Astrophys.* **281**, 923 (1994).
- [29] M. Steglich, C. Jäger, G. Rouillé, F. Huisken, H. Mutschke, and T. Henning, *ApJL* **712**, L16 (2010).
- [30] I. Garkusha, J. Fulara, P. J. Sarre, and J. P. Maier, *J. Phys. Chem. A* **115**, 10972 (2011).

- [31] R. Rodríguez-Cantano, R. P. de Tudela, M. Bartolomei, M. I. Hernández, J. Campos-Martínez, T. González-Lezana, P. Villarreal, J. Hernández-Rojas, and J. Bretón, *J. Chem. Phys.* **143**, 224306 (2015).
- [32] D. J. Wales and J. P. K. Doye, *J. Phys. Chem. A* **101**, 5111 (1997).
- [33] F. Pirani, S. Brizi, L. Roncaratti, P. Casavecchia, D. Cappelletti, and F. Vecchiocattivi, *Phys. Chem. Chem. Phys.* **10**, 5489 (2008).
- [34] F. Pirani, M. Albertí, A. Castro, M. M. Teixidor, and D. Cappelletti, *Chem. Phys. Lett.* **394**, 37 (2004).
- [35] M. Bartolomei, E. Carmona-Novillo, M. I. Hernández, J. Campos-Martínez, and F. Pirani, *J. Phys. Chem. C* **117**, 10512 (2013).
- [36] A. Griewank and A. Walter, *Evaluating Derivatives: Principles and Techniques of Algorithmic Differentiation* (Society of Industrial and Applied Mathematics, 2008).
- [37] K. T. Tang and J. P. Toennies, *J. Chem. Phys.* **118**, 4976 (2003).
- [38] Z. Li and H. A. Scheraga, *Proc. Natl. Acad. Sci. U.S.A* **84**, 6611 (1987).
- [39] J. Hernández-Rojas, F. Calvo, J. Bretón, and J. Gomez Llorente, *J. Phys. Chem. C* **116**, 17019 (2012).
- [40] S. Acosta-Gutiérrez, J. Bretón, J. M. G. Llorente, and J. Hernández-Rojas, *J. Chem. Phys.* **137**, 074306 (2012).
- [41] J. Hernández-Rojas, J. Bretón, J. M. Gomez Llorente, and D. J. Wales, *J. Phys. Chem. B* **110**, 13357 (2006).
- [42] J. P. K. Doye and D. J. Wales, *Phys. Rev. B* **59**, 2292 (1999).
- [43] J. Hernández-Rojas and D. J. Wales, *J. Chem. Phys.* **119**, 7800 (2003).
- [44] J. Hernández-Rojas, J. Bretón, J. M. Gomez Llorente, and D. J. Wales, *J. Chem. Phys.* **121**, 12315 (2004).
- [45] J. Hernández-Rojas, J. Bretón, J. G. Llorente, and D. Wales, *Chem. Phys. Lett.* **410**, 404 (2005).
- [46] J. Hernández-Rojas, F. Calvo, F. Rabilloud, J. Bretón, and J. M. Gomez Llorente, *J. Phys. Chem. A* **114**, 7267 (2010).
- [47] D. J. Wales, *Energy Landscapes* (Cambridge University Press, Cambridge, 2003).
- [48] Y. Kwon, D. M. Ceperley, and K. B. Whaley, *J. Chem. Phys.* **104**, 2341 (1996).
- [49] R. Rodríguez-Cantano, D. López-Durán, R. Pérez de Tudela, T. González-Lezana, G. Delgado-

- Barrio, P. Villarreal, and F. A. Gianturco, *Comp. Theor. Chem.* **990**, 106 (2012).
- [50] R. Rodríguez-Cantano, R. Pérez de Tudela, D. López-Durán, T. González-Lezana, F. A. Gianturco, G. Delgado-Barrio, and P. Villarreal, *Eur. Phys. J. D* **67**, 119 (2013).
- [51] R. Rodríguez-Cantano, T. González-Lezana, P. Villarreal, and F. A. Gianturco, *J. Chem. Phys.* **142**, 104303 (2015).
- [52] M. F. Herman, E. J. Bruskin, and B. J. Berne, *J. Chem. Phys.* **76**, 5150 (1982).
- [53] K. R. Glaesemann and L. E. Fried, *J. Chem. Phys.* **116**, 5951 (2002).
- [54] M. Sprik, M. Klein, and D. Chandler, *Phys. Rev. B* **31**, 4234 (1985).
- [55] E. Cuervo and P.-N. Roy, *J. Chem. Phys.* **125**, 124314 (2006).
- [56] R. Pérez de Tudela, D. López-Durán, T. González-Lezana, G. Delgado-Barrio, P. Villarreal, F. A. Gianturco, and E. Yurtsever, *J. Phys. Chem. A* **115**, 6892 (2011).
- [57] M. E. Tuckerman, *Statistical Mechanics: Theory and Molecular Simulation* (Oxford University Press, 2010).
- [58] M. I. Hernández, M. Bartolomei, and J. Campos-Martínez, *J. Phys. Chem. A* **119**, 10743 (2015).

Figures

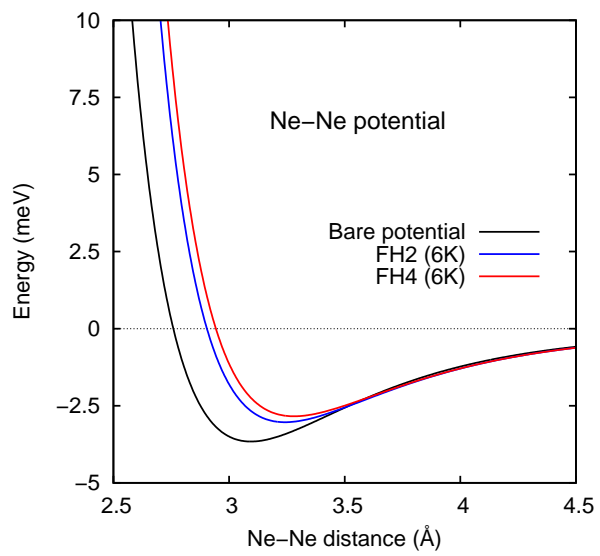


FIG. 1: Bare Ne-Ne interaction potential (meV) as a function of the interatomic distance (in Å), compared with the quadratic and quartic Feynman-Hibbs effective potentials at 6 K.

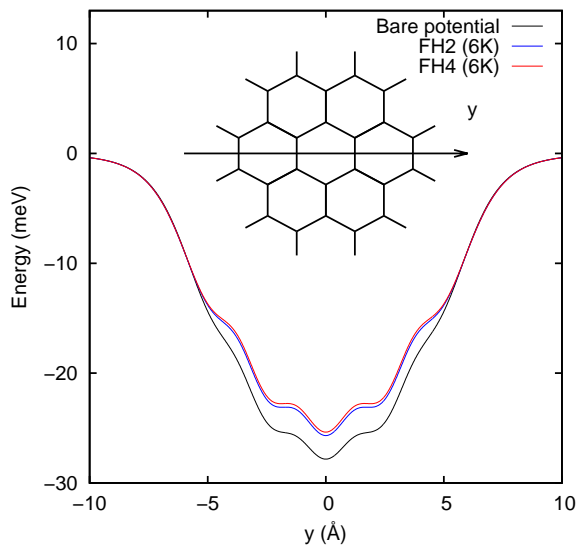


FIG. 2: Ne-coronene (Bare, FH2 and FH4 at 6K) interaction potentials (in meV), as functions of the y Cartesian coordinate (depicted in the inset), where the x and z coordinates are fixed at the absolute minimum of the bare potential (0. and 3.21 Å, respectively).

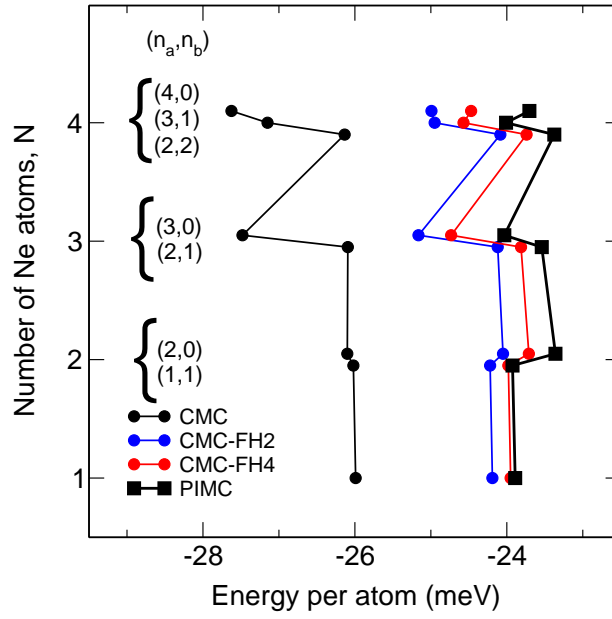


FIG. 3: Energies per atom (in abscissas) of Ne_N -coronene at 6 K as obtained from CMC, CMC-FH2, CMC-FH4 and PIMC, for the different sizes N and isomers (n_a, n_b) (in ordinates).

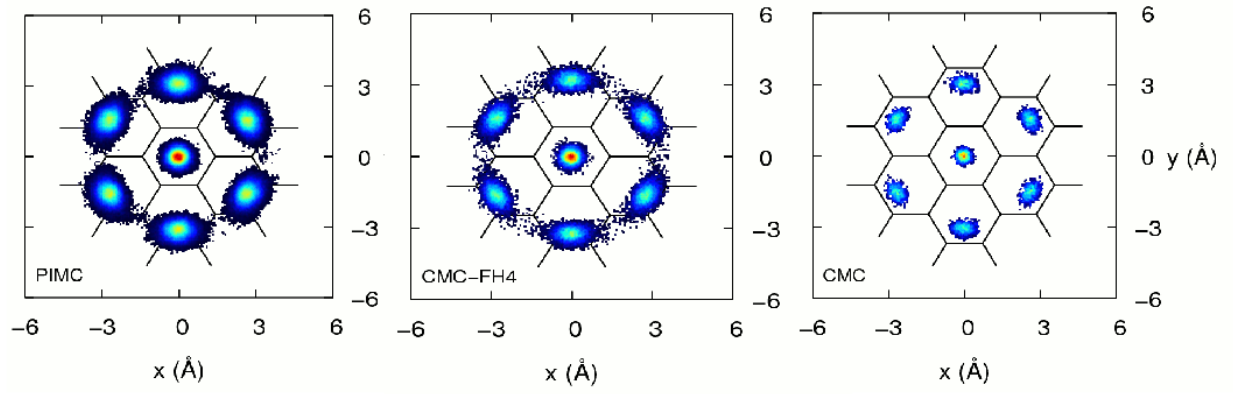


FIG. 4: Probability densities $\mathcal{D}(x, y)$ of (7,7) Ne₁₄-coronene at 6 K. Left, middle and right panels: PIMC, CMC-FH4 and CMC calculations, respectively.

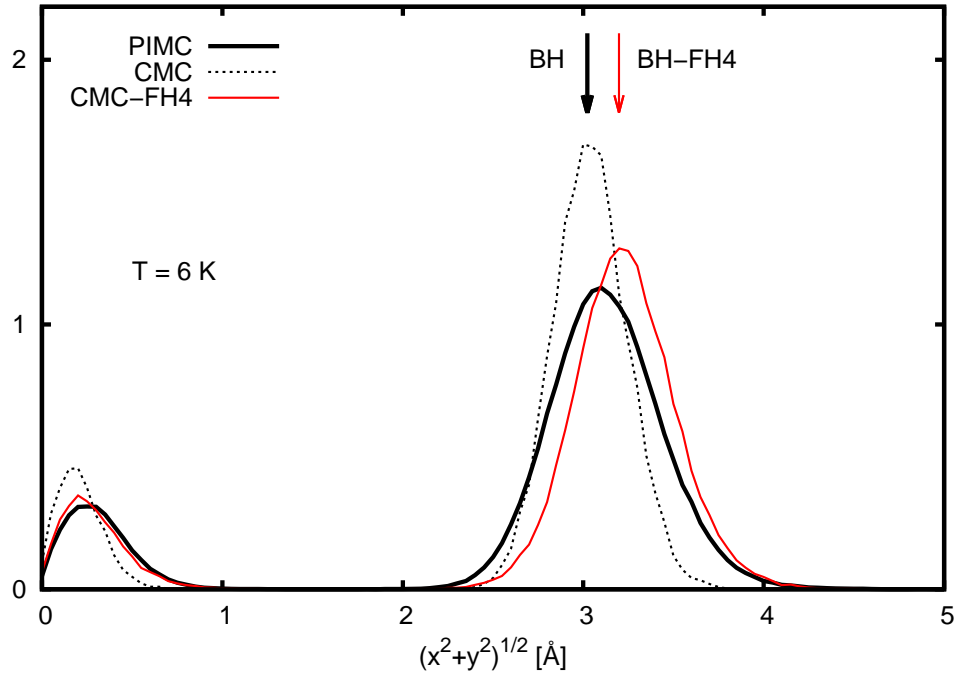


FIG. 5: Normalized probability density $\mathcal{D}([x^2 + y^2]^{1/2})$ of (7,7) Ne₁₄-coronene at 6 K, for CMC, CMC-FH4 and PIMC calculations. In addition, the distance of the outer Ne atoms to the coronene symmetry axis (z), as obtained from the BH and BH-FH4 calculations, are depicted by arrows.

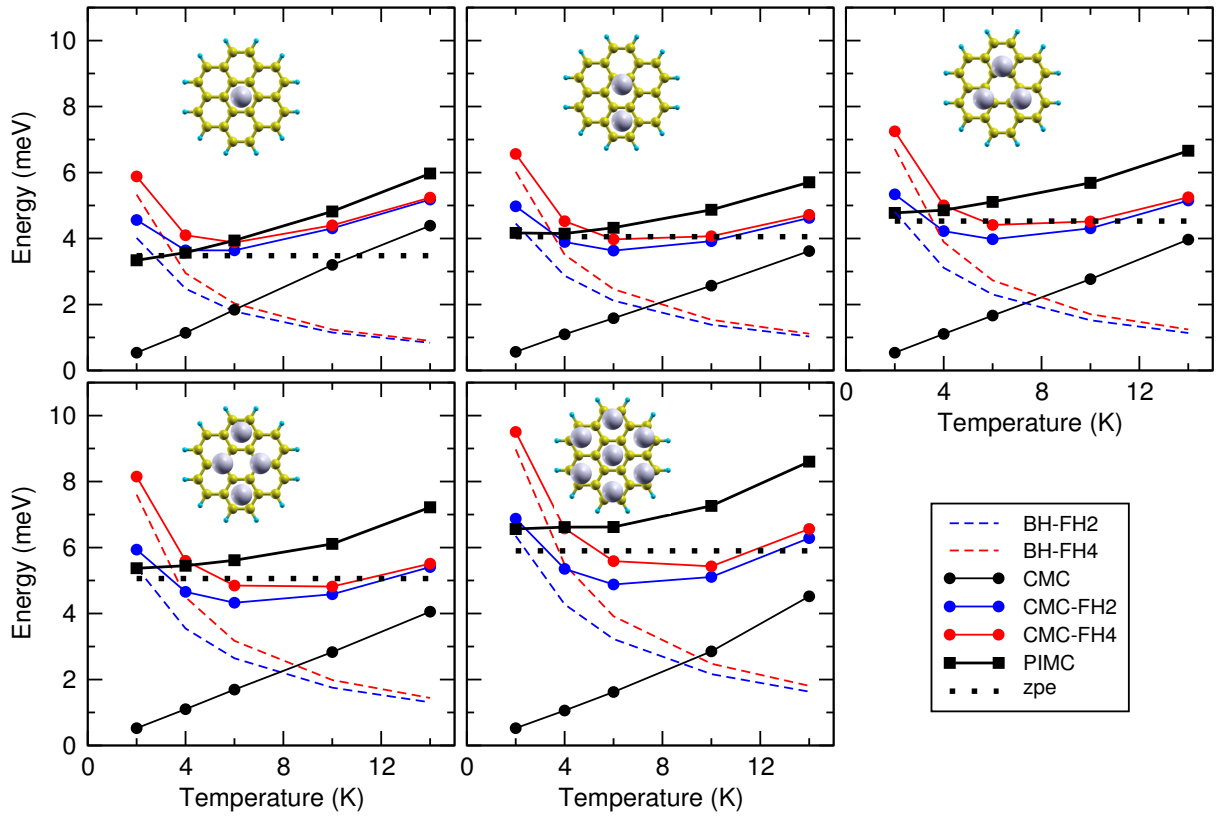


FIG. 6: Energies per atom, shifted as in Eq.15, of Ne_N -coronene clusters as functions of temperature for the different methods used in this work. Insets depict the classical optimal geometries of the clusters. (1,0), (2,0), (3,0), (4,0) and (7,7) are shown in the left upper, middle upper, right upper, left lower and middle lower panels, respectively. Calculations have been performed at 2, 4, 6, 10, and 14 K (lines are guides to the eye). See text for discussion.

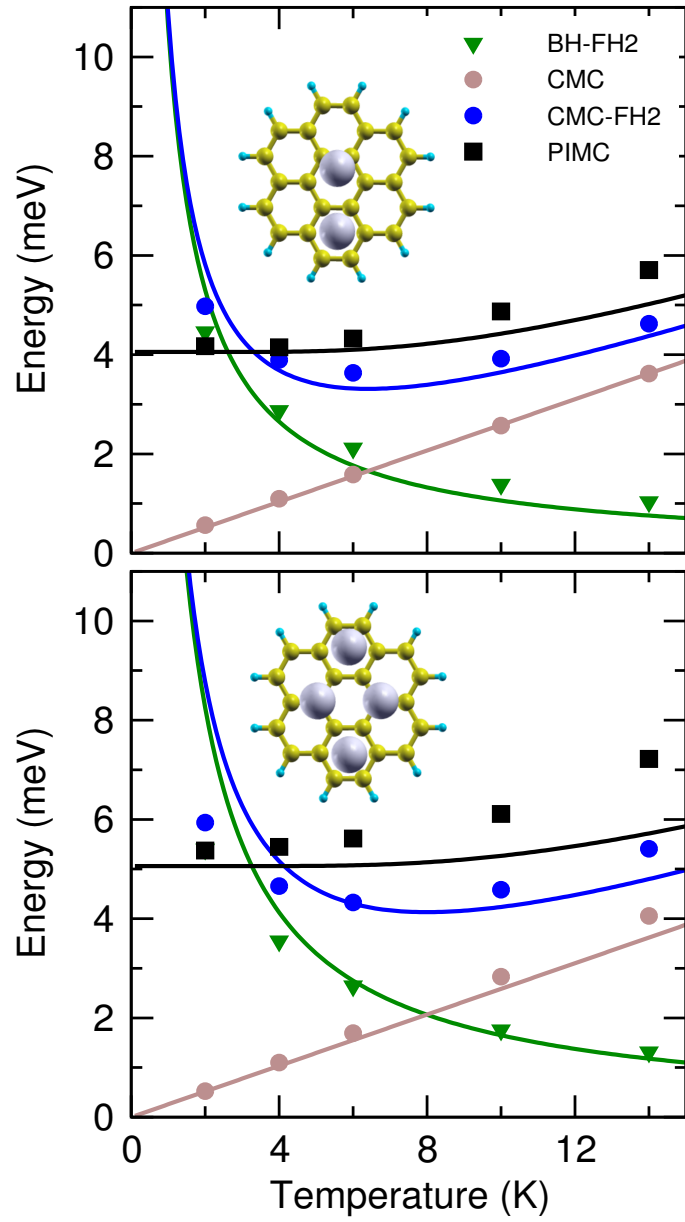


FIG. 7: Comparison between the computed BH-FH2, CMC, CMC-FH2 and PIMC energies (symbols) and the corresponding energies obtained with a model of N harmonic oscillators (solid lines). Upper and lower panels: (2,0) and (4,0) clusters, respectively. See text for details.

Tables

TABLE I: Parameters of the Ne-Ne, Ne-CC and Ne-CH pair potentials[33, 35]. Distances are in Å, energies in meV, and γ is dimensionless.

Pair	ρ_e	ε	γ		
Ne-Ne	3.094	3.660	9.0		
	ρ_e^\perp	ρ_e^\parallel	ε^\perp	ε^\parallel	γ
Ne-CC	1.297	1.809	3.643	3.995	8.5
Ne-CH	2.544	1.782	3.316	3.655	9.0

TABLE II: Ne_N -coronene energies (in meV) at 6 K for the different calculations of this work (see text for details). Various isomers (n_a, n_b) are studied, where n_a (n_b) is the number of Ne atoms above (below) the coronene plane. PIMC error bars (in meV), associated to the $M \rightarrow \infty$ extrapolation procedure, are given in parenthesis. Standard deviation of the CMC energies (not shown) is about 0.01 meV. For a given N , the absolute minimum energy within each method is shown in boldface.

N	(n_a, n_b)	BH	BH+ZPE	BH-FH2	BH-FH4	CMC	CMC-FH2	CMC-FH4	PIMC
1	(1,0)	-27.83	-24.35	-26.04	-25.80	-25.99	-24.19	-23.95	-23.89 (0.01)
2	(1,1)	-55.72	-48.75	-52.12	-51.65	-52.04	-48.44	-47.96	-47.85 (0.10)
	(2,0)	-55.36	-47.26	-51.13	-50.44	-52.20	-48.10	-47.42	-46.72 (0.03)
3	(3,0)	-87.42	-73.85	-80.51	-79.23	-82.44	-75.49	-74.20	-72.10 (0.01)
	(2,1)	-83.28	-71.69	-77.25	-76.32	-78.28	-72.36	-71.44	-70.62 (0.01)
4	(4,0)	-117.29	-97.03	-106.68	-104.58	-110.50	-99.97	-97.88	-94.81 (0.10)
	(3,1)	-115.38	-98.32	-106.66	-105.14	-108.60	-99.80	-98.28	-96.04 (0.20)
	(2,2)	-110.90	-94.66	-102.41	-101.01	-104.54	-96.34	-94.96	-93.50 (0.20)
14	(7,7)	-415.15	-332.53	-369.99	-360.34	-392.46	-346.83	-336.94	-322.44 (0.02)

TABLE III: Relative errors (in %) of the CMC energies with respect to the PIMC ones ($|E^{\text{CMC}} - E^{\text{PIMC}}| / E^{\text{PIMC}}$) as obtained from the different potentials and clusters (n_a, n_b) .

T (K)	Potential	(1,0)	(2,0)	(3,0)	(4,0)	(7,7)
	Bare	7	10	12	14	20
10	FH2	2	4	6	7	10
	FH4	2	4	5	6	8
